Journal of Molecular Liquids 363 (2022) 119868

Contents lists available at ScienceDirect

Journal of Molecular Liquids

journal homepage: www.elsevier.com/locate/molliq

Ion-pairing equilibria and kinetics of dimethyl phosphate: A model for counter-ion binding to the phosphate backbone of nucleic acids

Bence Kutus [a,b,*], Kenneth Wagner [a,c], Manfred Wagner [a], Johannes Hunger [a,*]

[a] Max Planck Institute for Polymer Research, Ackermannweg 10, D-55128 Mainz, Germany
[b] Institute of Chemistry, University of Szeged, Rerrich Béla tér 1, H-6720 Szeged, Hungary
[c] Faculty of Chemistry and Mineralogy, University of Leipzig, Johannisallee 29, D-04103 Leipzig, Germany

ARTICLE INFO

Article history:
Received 26 April 2022
Revised 28 June 2022
Accepted 14 July 2022
Available online 18 July 2022

Keywords:
Dimethyl phosphate
Nucleic acid
Ion pairing
Equilibrium
Kinetics
Dielectric relaxation spectroscopy

ABSTRACT

Dimethyl phosphate (DMP^-) is the simplest model ion to assess ion-pairing phenomena between metal ions and the phosphate backbone of nucleic acids. Yet, the equilibria and dynamics of ion binding to DMP^- have not been fully uncovered. Here, we study the interaction of DMP^- with different cations and water in aqueous solutions of NaDMP using dielectric relaxation and nuclear magnetic resonance spectroscopies. We find DMP^- to be weakly hydrated and weakly associated with Na^+ in the absence of added salt. Upon addition of NaCl, $MgCl_2$, or $CaCl_2$ to solutions of NaDMP, we detect the formation of solvent-shared ($NaDMP^0$) and contact ($MgDMP^+$, $CaDMP^+$) ion-pairs; the degree of ion association is 20–27 % at 2:1 salt:DMP molar ratio for the bivalent ions. Comparison to literature results suggests the formation constant of $MgDMP^+$ to be a good estimate for the binding of Mg^{2+} to RNA. From the concentration dependence of the rotational relaxation time of the ion-pairs, we find ion-pair dissociation rates to follow the order $Mg^{2+} \ll Ca^{2+} < Na^+$. Strikingly, our data suggest that the overall ion-pair dissociation dynamics are governed by an ion-pair metathesis reaction, which provides a different pathway for the binding of ions by DMP^-.

1. Introduction

In cells, alkali and alkaline earth metal ions (K^+, Na^+, Mg^{2+}, Ca^{2+}, etc.) condense around hydrated RNA and DNA, establishing an ion atmosphere [1]. This ionic environment is pivotal in stabilizing the macromolecular structure by compensating for the overall negative charge of the phosphodiester backbone [1–7]. As such, cation-nucleic acid interactions govern the functioning of nucleic acids and affect folding [3,5,8,9], enzymatic reactions [5,10,11], and protein binding [12].

The binding of metal ions to DNA, RNA and their fragments has been studied in great detail by applying X-ray crystallography [13–17], nuclear magnetic resonance (NMR) [14,18–20], infrared (IR)/Raman [20,21], fluorescence [21] spectroscopies, ion exchange [4,22], and molecular dynamics (MD) simulations [2,6,14,20–29]. From these studies, it has become apparent that divalent cations exhibit a higher affinity to phosphate oxygens, whereas monovalent ions are similarly attracted to phosphate groups and nucleobases [5,14,20–28]. Nevertheless, a large fraction of cations is expected to accumulate around the phosphate backbone due to its intrinsic negative charge. Indeed, MD simulations for different types of DNA have suggested preferential interaction of cations with the phosphate groups at bulk ion concentrations relevant for intracellular media [6,23].

Given the dominant role of the phosphate backbone in cation binding, characterizing the nature, strength, and dynamics of ion binding by phosphate is indispensable for understanding the nature of the ionic atmosphere around DNA or RNA. In general, cation-phosphate interactions are primarily governed by electrostatic forces, and they can occur as contact ion-pairs (CIP), where the phosphate group is located in the first solvation shell of the cation, or solvent-shared ion-pairs (SIP), where ions are separated by one solvent layer, or solvent-separated ion-pairs (SSIP), in which both ions retain a single solvation layer. The tendency of cations to bind to the phosphate backbone increases with increasing surface charge density of the cations: $Mg^{2+} \gtrsim Ca^{2+} \gg Na^+ \gtrsim K^+$ [4,6,17,20–22,28,30]. Also, stronger binding often results in slower dissociation dynamics [5,6,17,18,20,21,23,24,27,28]. In this respect, infrared experiments and ab initio molecular dynamics simulations have suggested that up to ~ 6 Mg^{2+} ions can form direct contacts to 11 different binding sites of tRNA with ion residence times longer than 1 μs [21].

* Corresponding authors.
E-mail addresses: kutusb@chem.u-szeged.hu (B. Kutus), hunger@mpip-mainz.mpg.de (J. Hunger).

https://doi.org/10.1016/j.molliq.2022.119868
0167-7322/

However, it is challenging to quantitatively generalize such findings since these interactions strongly depend on several factors, including the bulk concentration of ions, the phosphate backbone's direct environment, and the macromolecule's hydration state. Therefore, low-molecular-weight phosphate diesters are often used to assess phosphate-specific ion binding, which in turn helps disentangle ion-nucleic acid interactions in a more complex molecular environment. In this regard, dimethyl phosphate has become a well-established model compound and its association with Ca^{2+}, Mg^{2+} and Na^+ ions in aqueous solutions has been studied using a range of experimental and computational methods [31–44]. Raman and infrared (IR) spectra of DMP^- in the presence of excess Mg^{2+}, Ca^{2+} or Na^+ ions [39,43,44] have shown that both, symmetric and asymmetric, stretching vibrations of DMP^- undergo a pronounced blue-shift upon addition of these cations, which has been ascribed to the formation of CIPs with 1:1 stoichiometry. The magnitude of the blue-shift follows the order $Mg^{2+} > Ca^{2+} > Na^+$, implying the same order of binding strengths. Indeed, quantitative analysis of IR spectra yielded the stability trend for CIPs as $Mg^{2+} \gtrsim Ca^{2+} \gg Na^+$, in agreement with a previous ^{31}P NMR study [31], albeit the type of IP has not been specified. In addition to CIPs, the formation of SIPs (or SSIPs) to a minor degree has also been inferred from vibrational spectra [39,43,44]. Contrary to these results, computational studies have suggested SIP to be the predominant IP species for Mg^{2+} and Na^+ [29,35–37,40]. As for the kinetics of ion pairing, the information is scarce and only a lower limit of ~ 1 μs has been inferred for the lifetime of Mg^{2+} IPs [21], while Ca^{2+} IPs have been suggested to form and dissociate on the ps time-scale [38].

As such, the nature of the prevailing IPs for a given metal ion in equilibrium is not fully settled, and ion-pair formation constants have been determined at rather different ionic strengths. Given that the ionic strength markedly affects ion pairing (due to charge screening), a direct comparison of the stabilities of different IPs is therefore challenging. To better compare IP stabilities, in particular for mono- and divalent cations, the determination of the standard association constants at infinite dilution is required.

Herein, we study the ion association between DMP^-, and Mg^{2+}, Ca^{2+}, or Na^+ ions in aqueous solution using dielectric relaxation spectroscopy (DRS), which can detect different ion-pair species (CIP, SIP, or SSIP) via their dipolar rotational dynamics [45–47]. From the dielectric results we find the IP lifetimes to be close to their rotation time and we determine the kinetics of IP formation and dissociation. To assign the observed species we compare our results to ^{31}P NMR experiments: We find the predominant IP to be CIPs for Mg^{2+} and Ca^{2+}, whereas SIPs prevail in the presence of Na^+. The determined IP standard association constants for Ca^{2+} and Mg^{2+} are markedly higher than for Na^+. A comparison of our results to the binding of Mg^{2+} to tRNA suggests that the binding of ions to RNA can be estimated well using the association constants with DMP^-, reinforcing that DMP^- is an insightful model to assess ion pairing with the phosphate backbone.

2. Materials and methods

2.1. Sample preparation

NaCl (a.r. grade, Carl Roth), $CaCl_2{\cdot}2H_2O$ (≥99.0 %, Sigma-Aldrich), $MgCl_2{\cdot}6H_2O$ (ACS grade, VWR), trimethyl phosphate (≥99.0 %, Sigma-Aldrich) and sodium dimethyl phosphate (NaDMP, 93 %, Toronto Research Chemicals) were used as received. Analysis of the impurities in NaDMP revealed ethyl methyl phosphate as the major impurity, amounting to ~ 7 %. (For the details of the analysis, see the discussion in the Supporting Information (SI) and Figures S1–S3). Due to the structural similarity of this compound to DMP^-, we treated this impurity as DMP^-.

We prepared solutions with varying concentrations of NaDMP and solutions of 0.2 M NaDMP with different concentrations of $MgCl_2$, $CaCl_2$, or NaCl. The composition of all samples is listed in Tables S1–S4 in the SI. The metal-ion content for $CaCl_2{\cdot}2H_2O$ and $MgCl_2{\cdot}6H_2O$ was determined by complexometric titrations using $Na_2EDTA{\cdot}2H_2O$ (a.r. grade, Thermo Fisher Scientific) as titrant. The pH of solutions of NaDMP (c_{NaDMP} = 0.03–0.3 M) was measured to be 7.5–9.3, consistent with the anionic form of DMP prevailing in solution (the pK_a of dimethylphosphoric acid is 1.29 [48]). All samples were prepared by dissolving the salts in Milli-Q water (Merck Millipore, Ω = 18.6 S cm^{-1} at 25 °C) or in D_2O (99.9 atom % D, Sigma-Aldrich) in 1 or 5 mL volumetric flasks with a volume error of ± 2.5 % or ± 0.5 %, respectively.

2.2. Dielectric spectroscopic measurements

DRS probes the macroscopic polarization of a sample in an external oscillating electric field as a function of frequency, ν, by recording the complex permittivity, $\hat{\varepsilon}(\nu)$:

$$\hat{\varepsilon}(\nu) = \varepsilon\prime(\nu) - i\varepsilon\prime\prime(\nu) \quad (1)$$

where $\varepsilon'(\nu)$ and $\varepsilon''(\nu)$ are the frequency-dependent dielectric permittivity and loss, respectively [49]. For liquids, orientational polarization processes due to the motion of species with a permanent electric dipole are typically observed at microwave frequencies. At low frequencies, the molecular ensemble can rearrange according to the oscillating electric field, giving rise to a polarization as measured by ε'. With increasing frequency, molecules cannot follow the alternating field, resulting in a decrease in ε' and a peak in ε". For electrolyte solutions, an additional low-frequency Ohmic loss is observed, associated with the ionic polarization due to translational motions of mobile ions.

In this work, $\hat{\varepsilon}(\nu)$ spectra were recorded at 0.25 GHz < ν < 125 GHz using an Anritsu vector network analyzer (VectorStar MS4647A). Frequencies at 0.25 GHz < ν < 50 GHz were covered using a frequency-domain reflectometer, using an open-ended coaxial probe based on 1.85 mm connectors. Experiments at 50 GHz < ν < 125 GHz were carried out using an open-ended probe, connected with 1 mm connectors to an external frequency converter module (Anritsu 3744A mmW) [50]. To calibrate the setup, air, conductive silver paint, and H_2O [51] were used as calibration standards. All measurements were performed at room temperature ((21 ± 1) °C).

2.3. Nuclear magnetic resonance spectroscopic experiments

Proton-decoupled ^{31}P NMR spectra were acquired using a Bruker Avance 300 MHz spectrometer. The samples were placed into a quartz tube containing a sealed capillary with 0.5 M trimethyl phosphate in D_2O. For each spectrum, 32 interferograms were collected. The obtained chemical shifts were then referenced by setting the ^{31}P chemical shift of trimethyl phosphate to 3 ppm [31]. All spectra were measured at (25 ± 2) °C.

For assigning impurities in NaDMP additional ^1H (16 scans), ^{31}P (256 scans) and ^1H–^{31}P heteronuclear multiple bond correlation (HMBC) spectra were recorded for a 0.2 M NaDMP solution in D_2O, using a Bruker Avance III Topspin 3.5 500 MHz spectrometer. The HMBC spectrum was obtained applying 0.5849 s acquisition time and 4.0000 s relaxation delay time, and setting the long-range coupling constant to 5.0 Hz.

2.4. Quantum chemical calculations

The structure of the DMP^- anion was optimized at the M06-2X/def2–TZVPD level of theory [52,53], including Grimme's D3 dispersion correction [54], using the Gaussian 09 software [55]. We used the gauche-gauche, trans-gauche, and trans–trans conformer [33,34,36,41] as starting geometries. Solvent effects were modeled using the conductor-like polarizable continuum model [56] with H_2O as solvent. Geometry optimization and subsequent single-point energy calculations yielded the gauche-gauche conformation (Fig. 1) to be energetically most favorable, in agreement with Ref. [34]. Other conformations are shown in Figure S4, SI. The dipole moment and polarizability of the gauche-gauche anion – required for the evaluation of the DR spectra – were determined to be 8.78 D and 12.38 $Å^3$, respectively.

3. Results and discussion

3.1. Qualitative analysis of the dielectric spectra

Before studying the effect of added salts to solutions of NaDMP, we first analyze the dielectric spectra of neat NaDMP solutions, where weak ion pairing between Na^+ and DMP^- ions has already been suggested based on NMR measurements [31]. Fig. 2a shows the dielectric spectra of aqueous solutions of NaDMP at concentrations ranging from c_{NaDMP} = 0.05 to 0.30 M. All spectra exhibit a high static permittivity and an intense loss peak at ~ 20 GHz, common to spectra for water and aqueous solutions [51,57–61]. Upon addition of salt, we observe the static permittivity, ε_s (low-frequency plateau of ε') and ε'' at the absorption maximum (~20 GHz) to decrease. Such so-called depolarization stems predominantly from dilution: the addition of salt to a given volume of water dipoles reduces their concentration, hence ε_s and ε'' decrease, as both quantities scale with the volume concentration of the rotating dipoles. Furthermore, binding of water in the ions hydration shells [57,59], kinetic depolarization due to the coupling between the translation of ions and the reorientation of dipolar water [62], or salt-induced changes to the correlated motion of water dipoles [63,64] can contribute to the observed depolarization.

This depolarization is most apparent from the differential fitted ε'' spectra relative to that of water [51] in Fig. 2b ($\varepsilon''_{NaDMP}(\nu) - \varepsilon''_{water}(\nu)$, for details on fitting the experimental spectra, see the next section), which show a marked negative peak at ~ 20 GHz. Interestingly, we find an increase in ε'' at ~ 2 GHz with increasing c_{NaDMP} (Fig. 2b). As such, the differential spectra provide evidence for the contribution of (at least) two relaxation processes to the spectra: a solute mode (at ~ 2 GHz) that increases in amplitude with increasing c_{NaDMP} and a solvent mode (at ~ 20 GHz) with decreasing amplitude. Upon addition of NaCl, $MgCl_2$, or $CaCl_2$ to solutions of NaDMP we observe the same qualitative trends (see Figures S5–S7, SI), suggesting that the same relaxation modes contribute to the spectra with added salt.

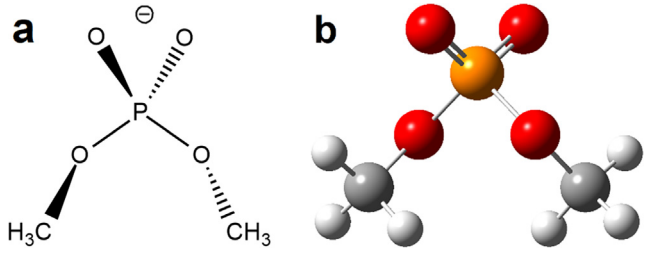

Fig. 1. Structure of dimethyl phosphate (DMP^-) in gauche-gauche conformation: (**a**) perspective drawing, (**b**) ball-and-stick representation as obtained from geometry optimization at the M06-2X–D3–CPCM/def2-TZVPD level of theory.

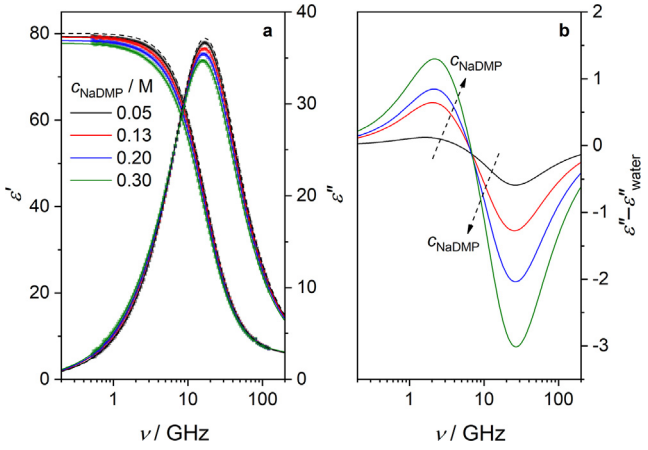

Fig. 2. (**a**) Relative permittivity (ε', left axis) and dielectric loss spectra (ε'', right axis) of selected NaDMP solutions, corrected for Ohmic loss contributions (last term of Eq. (2)). Symbols refer to experimental data, solid lines are the results of fitting Eq. (2) to the data, and the dashed line shows the spectrum of neat water, taken from Ref. [51]. (**b**) Calculated differential loss spectra, $\varepsilon''_{NaDMP}(\nu) - \varepsilon''_{water}(\nu)$, based on the fits in panel a). The dashed arrows indicate increasing c_{NaDMP}.

3.2. Relaxation model and assignment of the relaxation processes

To quantify the contributions of the solvent and the solute to the spectra, we tested different relaxation models based on a sum of symmetrically and asymmetrically broadened Havriliak–Negami modes [65] to model the experimental $\hat{\varepsilon}(\nu)$ spectra. For all samples, a relaxation model consisting of two Debye modes and one Cole-Cole mode – both being simplified versions of the Havriliak–Negami model – provided the lowest reduced error functions [65] with the least number of adjustable parameters:

$$\hat{\varepsilon}(\nu) = \frac{S_1}{1 + i2\pi\nu\tau_1} + \frac{S_2}{1 + (i2\pi\nu\tau_2)^{1-\alpha}} + \frac{S_3}{1 + i2\pi\nu\tau_3} + \varepsilon_\infty - i \times \frac{\kappa}{2\pi\nu\varepsilon_0} \quad (2)$$

where S_j are the relaxation amplitudes, τ_j are the relaxation times, and α is the Cole-Cole parameter. ε_∞ is the infinite-frequency permittivity, which comprises all high-frequency polarization contributions. The static permittivity, ε_s, equals $S_1 + S_2 + S_3 + \varepsilon_\infty$. The last term of Eq. (2) accounts for the Ohmic loss contribution due to the conductivity, κ, which we assume to be real and independent of frequency (dc conductivity); ε_0 is the permittivity of free space.

Here, the first relaxation mode (τ_1, S_1) accounts for the solute mode at ~ 2 GHz, as discussed above. The Cole-Cole process (τ_2, S_2, α) models the collective relaxation of the hydrogen-bonded water [57,60]. We find the water relaxation for solutions of NaDMP/NaCl to be slightly symmetrically broadened ($\alpha > 0$), which is common to the relaxation of NaCl solutions [59]. For aqueous NaDMP solutions with $MgCl_2$ and $CaCl_2$, a Debye-type ($\alpha = 0$) for the second mode provides satisfactory fits to the experimental data. For the Mg^{2+}/Ca^{2+} samples, this model is somewhat unexpected as the solvent mode has been found to be a Cole-Cole-type for neat $MgCl_2$ and $CaCl_2$ solutions [58,61]. Nevertheless, such broadening described by $\alpha > 0$ becomes significant only at higher concentrations ($c_{salt} \geq 0.5$ M), which explains why a Debye relaxation suffices for our samples ($c_{salt} \leq 0.4$ M). The highest-frequency relaxation (τ_3, S_3) is also commonly observed for water and aqueous solutions [57,61,66–68]. This weak (low amplitude)

relaxation has been related to fast reorientational dynamics of water and translational relaxation of ions [57,60,61,66–68]. Given its low amplitude and considering that our frequency window covers this relaxation only partly, we refrain from a detailed discussion. To limit the number of adjustable parameters associated with this relaxation, we constrain ε_∞ and τ_3 to the values found for neat water [51], as both, S_3 and τ_3, are little affected by salts [61].

The contributions of these relaxation modes to the dielectric loss spectra for a 0.2 M solution of NaDMP are exemplarily displayed in Fig. 3. Typical fits for the NaDMP-containing samples are shown in Fig. 2a and in Figures S5–S7, SI. Fits for neat NaCl, $MgCl_2$ and $CaCl_2$ solutions are discussed in the SI. To evaluate the reproducibility of our measurements, we measured the NaDMP/NaCl samples twice; the average deviations between the parameters are as follows: ε_s: 0.3 %, S_1: 12 %, S_2: 0.5 %, S_3: 3.7 %, τ_1: 11 %, τ_2: 0.6 %, α: 17 %, κ: 1.1 %. The fitted parameters are listed in Tables S1–S4, SI.

3.3. The structure and hydration of DMP^- in solution

To gain insights into the hydration of the DMP^- anion, we quantitatively analyze the parameters for relaxation mode of the solvent: We determine the effective number of water molecules that are bound to NaDMP such that they do not contribute to the dielectric spectra. This is achieved by correcting the relaxation amplitude of bulk water, $S_b = S_2 + S_3$ [69] for kinetic depolarization [70]. Based on the approach detailed in Ref. [69], we correct S_b for this effect as described previously [62], assuming Na^+ to be hydrated (i.e., we use $r_{Na+} + r_{H2O}$ for the effective radius for the cation). The radii of Na^+ (1.02 Å), H_2O (1.425 Å), were taken from literature [71,72], and the radius of DMP^- (3.42 Å) was determined from its diffusivity as obtained from diffusion-ordered NMR, assuming a spherical shape for the anion [73].

The thus corrected values of S_b can be related to the equilibrium concentration of the relaxing species X, [X], via [47]:

$$S = \frac{\varepsilon_s}{\varepsilon_s + A(1-\varepsilon_s)} \cdot \frac{[\mathrm{X}]\mu^2 N_\mathrm{A}}{3k_\mathrm{B}T\varepsilon_0} \tag{3}$$

where N_A is the Avogadro constant, k_B is the Boltzmann constant, T is the thermodynamic temperature, and A is the cavity-field factor, which is 1/3 for spherical species. Assuming the dipole moment of water and dipolar correlations in solution to be the same as in neat water, we take the effective dipole moment of water from the spectra of neat water (3.86 D [47]).

From Eq. (3), we obtain accordingly the equilibrium concentration of water, $[H_2O]$, i.e. the apparent concentration of water that contributes to the observed relaxation with relaxation amplitude S_b. The difference between $[H_2O]$ and the analytical concentration of water, c_{H2O}, yields the concentration of hydrating water molecules that do not contribute to the water relaxation owing to strong ion–dipole interactions [47]. The number of such dynamically 'frozen' solvent molecules per NaDMP, Z_{NaDMP},:

$$Z_{\mathrm{NaDMP}} = \frac{c_{\mathrm{H_2O}} - [\mathrm{H_2O}]}{c_{\mathrm{NaDMP}}} \tag{4}$$

is displayed in Fig. 4a, together with the hydration numbers of Na^+ [59]. The average values for Z_{NaDMP} = 7 ± 1 is rather similar to the value reported for NaCl (5.2 ± 0.4, at infinite dilution), in view of the associated uncertainties. Consequently, the detected hydration numbers for NaDMP can be largely attributed to bound water in the hydration shell of Na^+. In turn, DMP^- is weakly hydrated, which is in line with an earlier report on the structurally similar dihydrogen phosphate anion [74]. Overall, our findings indicate the relaxation dynamics of water in the hydration shell of DMP^- to be similar to that in the bulk.

Despite DMP^- weakly affects the relaxation of water, the addition of NaDMP gives rise to the emergence of the lowest-frequency relaxation (mode 1). Both, dipolar rotation of the non-centrosymmetric DMP^- anions and the formation of ion-pairs are conceivable molecular origins of the detected relaxation. To elucidate the molecular origin of mode 1, we analyze the relaxation parameters of this relaxation in more detail. The relaxation amplitudes, S_1, scale nearly linearly with c_{NaDMP} (Figure S8, SI), which would be expected (cf. Eq. (3)) for the rotation of the dipolar anion. To quantify the contribution of DMP^-, we determine the effective dipole moment of the solute species, μ_1, by inserting S_1 and c_{NaDMP} into Eq. (3) (assuming A = 1/3). Fig. 4b shows that the thus obtained values of μ_1 are very close to the value of the anions dipole

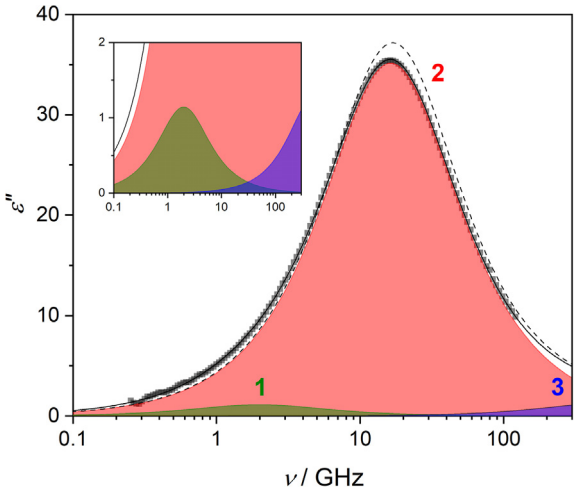

Fig. 3. Dielectric loss spectrum (ε'') of a 0.2 M NaDMP solution, corrected for Ohmic loss (Eq. (2)). Squares refer to the experimental data; the black solid line is the result of fitting Eq. (2) to the data, and the dashed line is the loss spectrum of neat water, taken from Ref. [51]. Shaded areas show the contribution of relaxation modes 1–3 to ε''. The inset shows a zoom for better visualization of modes 1 and 3.

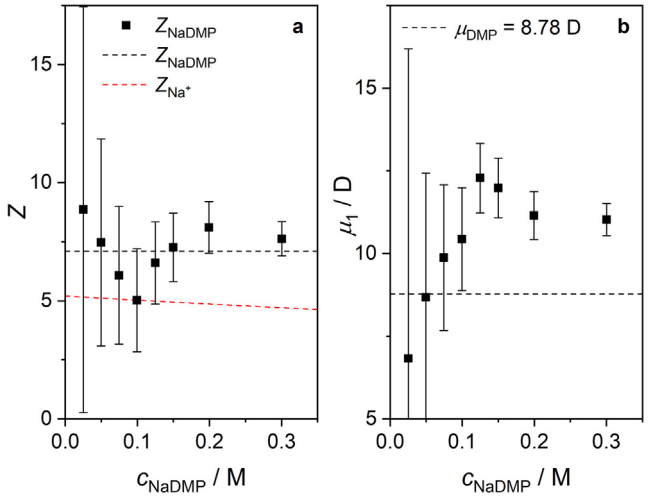

Fig. 4. (a) Hydration number (Z_{NaDMP}) of NaDMP, calculated using Eqs. (3) and (4) (symbols) and their average values (black dashed line). Also shown are the Z_{Na+} values for the Na^+ ion reported in Ref. 59 (red dashed line). **b)** Effective dipole moment for the solute mode 1 of NaDMP solutions, as obtained from Eq. (3) (symbols). Also shown is μ of the DMP^- ion in gauche-gauche conformation, as determined from DFT calculations (dashed line). Error bars were obtained assuming $\delta S = \pm 0.3$ for the relaxation amplitudes.

moment in gauche-gauche conformation (8.78 D), as determined from DFT calculations. This agreement provides experimental evidence for the gauche-gauche conformation to prevail in solution. At c_{NaDMP} > 0.1 M μ_1 moderately increases to 11–12 D. This increase might hint at the formation of ion-pairs between Na^+ and DMP^-, since the charge separation in such IPs is higher than in the anion, i.e. $\mu_{IP} > \mu_{DMP}$. However, given the modest increase in μ_1 with concentration and the experimental uncertainty of the extracted dipole moments, we do not analyze this increase further; rather we use the samples with added salts to identify the formation of ion pairs in the followings.

3.4. Ion pairing in the presence of NaCl, $MgCl_2$, or $CaCl_2$

To elucidate ion pairing with DMP^-, we study binary salt systems containing NaDMP with added NaCl, $MgCl_2$, or $CaCl_2$ at c_{salt}/c_{NaDMP} molar ratios of 1–10 (Na^+) or 0.2–2 (Mg^{2+}, Ca^{2+}). Upon addition of NaCl to a 0.2 M solution of NaDMP, S_1 initially increases up to c_{NaCl} = 0.6–0.8 M after which it decreases with increasing concentration (Fig. 5a). The initial increase may be explained by enhanced IP formation in the presence of NaCl. The decrease at elevated concentrations is commonly observed for ion pairing due to electrostatic screening or a concomitant reduction of the IP lifetime [45] (see also discussion below). Conversely, the addition of $MgCl_2$ and $CaCl_2$ to the NaDMP solution results in a monotonic increase in S_1 (Fig. 5b), indicative of increased formation of IPs. We note that for all three salts, also in the absence of NaDMP a solute relaxation mode is present, which has been reported to stem from the formation of 1:1 SSIPs of the chloride salts, i.e. $NaCl^0$, $MgCl^+$, $CaCl^+$ [59,69,75]. Due to the lower ionic radius of Cl^- as compared to DMP^-, and the resulting lower dipole moments the contribution of chloride IPs to the dielectric spectra is expected to be lower. Thus, we do not account for these solution species. Nevertheless, neglecting them may result in an over-estimation of ion pairing with DMP^-; yet, a comparison of the dielectric results to the NMR experiments (see discussion below) suggests that this overestimation is minor.

For quantitative analysis of the solute mode in the binary salt systems, we account for the relaxation of both the dipolar DMP^- anion and dipolar ion-pairs, contributing to the solute relaxation. Analogously to Eq. (3), we relate the experimental relaxation amplitudes the underlying molecular species:

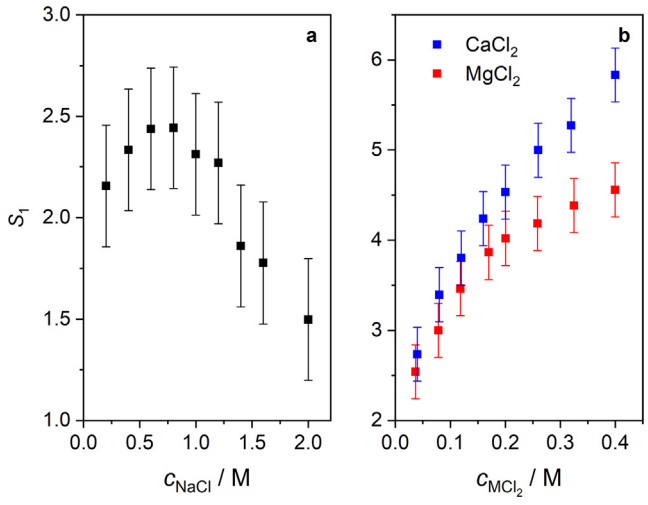

Fig. 5. Relaxation amplitudes of the solute mode 1 (S_1) as a function of concentration of (**a**) NaCl (average of two data sets) and **b**) $MgCl_2$ and $CaCl_2$ in the presence of 0.2 M NaDMP. Error bars represent δS_1 = ±0.3.

$$S_1 = \frac{N_A}{3k_BT\varepsilon_0}\left(\frac{\varepsilon_s}{\varepsilon_s + A_{DMP}(1-\varepsilon_s)}\cdot[DMP]\mu_{DMP}{}^2 + \frac{\varepsilon_s}{\varepsilon_s + A_{IP}(1-\varepsilon_s)}\cdot[IP]\mu_{IP}{}^2\right) \quad (5)$$

where the equilibrium concentrations of DMP^- and IPs are referred to as [DMP] and [IP], respectively. To obtain these concentrations, the corresponding dipole moments and shape factors, μ_{DMP}, A_{DMP}, μ_{IP} and A_{IP}, are required. We assume the anion to be spherical [73], hence A_{DMP} = 1/3 [65], and μ_{DMP} = 8.78 D (obtained from DFT calculations). A_{IP} and μ_{IP} depend on the geometry of the IP and the distance between the ions, which are however not directly accessible from the DR data. Thus, we consider the formation of three conceivable IP species: CIP, SIP, and SSIP [46,47,72]. For all three ion-pair species, we obtain μ_{IP} and A_{IP} based on the geometric model described in detail elsewhere [72,76], assuming the center of hydrodynamic stress as the pivot point. To this end, we use literature values for the ion/solvent radii (Na^+: 1.02 Å, Mg^{2+}: 0.72 Å, Ca^{2+}: 1.00 Å, DMP^-: 3.42 Å, H_2O: 1.425 Å) and polarizabilities (Na^+: 0.211 Å^3, Mg^{2+}: 0.111 Å^3, Ca^{2+}: 0.63 Å^3, H_2O: 1.444 Å^3) [71–73]. For the polarizability of DMP^-, we use the DFT value 12.38 Å^3 (details are listed in Table S5, SI).

Assuming the exclusive formation of CIP, SIP, or SSIP, we determine their equilibrium concentrations according to Eq. (5). Given the marked increase of the IP dipole moments with increasing counter-ion separation (SSIP > SIP > CIP, see Table S5, SI), the equilibrium concentrations as determined using Eq. (5) markedly depend on the assumed nature of the IP: [SSIP] < [SIP] < [CIP]. From these values, we determine the formation constants, K, as:

$$M + DMP \rightleftharpoons IP \quad (6)$$

$$K = \frac{[IP]c^{\varnothing}}{[M][DMP]} = \frac{[IP]c}{(c_{salt} + nc_{NaDMP} - [IP])(c_{NaDMP} - [IP])} \quad (7)$$

where [M] and [DMP] are the equilibrium concentrations of the metal ion and anion, respectively (charges omitted for convenience). c^o is the standard molar concentration (1 M), n is 1 for NaCl and 0 for $MgCl_2$ and $CaCl_2$. Together with the law of mass conservation (c_{NaDMP} = [DMP] + [IP], $c_{salt} + nc_{NaDMP}$ = [M] + [IP]), Eq. (7) allows for determining $\log K$ as a function of salt concentration. Fig. 6a-c show the thus obtained constants with the different IP species. We note that assuming the formation of CIP upon addition of NaCl results in [IP] > [DMP] in some cases, thus we disregard the formation of this species. From this analysis, it becomes apparent that the $MgDMP^+$ and $CaDMP^+$ ion-pairs are more stable (similar for Mg^{2+} and Ca^{2+}) as compared to the $NaDMP^0$ species, assuming the same ion-pair nature (e.g. SIP) to be exclusively formed.

To determine which IP species prevails in solution, we compare the thus obtained $\log K$ values to those determined by NMR: We measure the ^{31}P chemical shifts of DMP^- [31] as a function of c_{salt} using the same samples studied by DRS. Upon salt addition, we observe the chemical shift of DMP^- to shift upfield, suggesting that NMR detects the motionally averaged signal of all DMP^- in solution (i.e. fast exchange between free DMP^- and IPs on the NMR timescale) [31]. Accordingly, the measured chemical shift, δ, can be expressed as the concentration-weighted average of the chemical shift of DMP^-, δ_{DMP}, and IPs, δ_{IP}:

$$\delta = \delta_{DMP}\frac{[DMP]}{c_{NaDMP}} + \delta_{IP}\frac{[IP]}{c_{NaDMP}} \quad (8)$$

We find that assuming the formation of 1:1 IPs describes the variation of δ with added salt very well (see Figure S9, parameters of the fits are listed in Table S6, SI) and the obtained formation constants agree well with the results of an earlier NMR study [31] (see Table 1).

Comparison of the NMR constants with those obtained from DRS in the studied concentration ranges shows good agreement

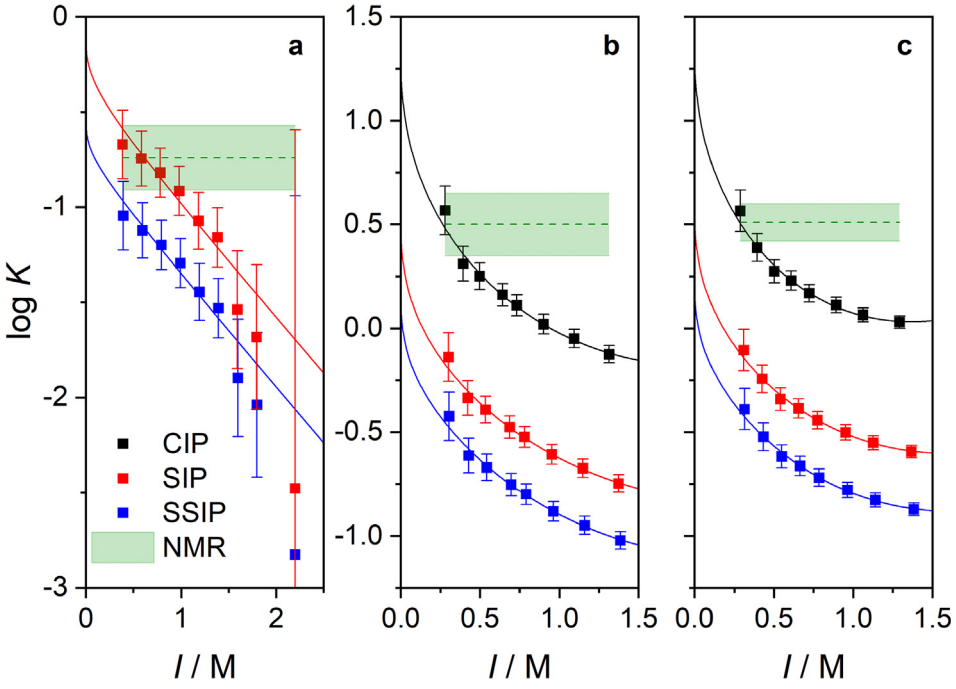

Fig. 6. Calculated ion-pairing equilibrium constants (log K) as a function of ionic strength (I) for **a)** $NaDMP^0$ (average of two data sets), **b)** $MgDMP^+$ and **c)** $CaDMP^+$ ion-pairs (IPs) in the presence of 0.2 M NaDMP. Symbols refer to values calculated from the solute amplitudes (S_1) via Eqs. (5) and (7), assuming the formation of contact (CIP), solvent-shared (SIP) or solvent-separated (SSIP) IPs. The error bars were obtained assuming $\delta S_1 = \pm 0.3$. Solid lines are the results of fitting Eq. (9) to the data. The dashed lines and shaded areas correspond to log $K \pm \delta$(log K), as determined from the ^{31}P chemical shift experiments (Eqs. (7) and (8)).

Table 1
Formation constants (log K) of contact (CIP) or solvent-separated ion-pairs (SIP) for Na^+, Mg^{2+}, or $Ca^{2+}$with DMP^- as determined from DRS or NMR experiments.

IP	Type of IP	log K^{0a}	log K^b	Method / Ref.
$NaDMP^0$	SIP	−0.11 ± 0.08		DRS / p. w.
			−0.74 ± 0.17	NMR / p. w.
			−0.54 ± 0.03	NMR / [31]
$MgDMP^+$	CIP	1.31 ± 0.08		DRS / p. w.
			0.50 ± 0.15	NMR / p. w.
			0.56 ± 0.01	NMR / [31]
$CaDMP^+$	CIP	1.34 ± 0.06		DRS / p. w.
			0.51 ± 0.09	NMR / p. w.
			0.60 ± 0.10	NMR / [31]

[a] Thermodynamic constants extrapolated to infinite dilution, corresponding to (21 ± 1) °C.
[b] Association constants determined at finite salt concentration at (25 ± 2) °C (p. w.) or (21 ± 1) °C (Ref. 31).

for solvent-shared $NaDMP^0$ and contact $MgDMP^+$/$CaDMP^+$ ion-pairs, respectively. As such, our data suggest that SIPs prevail for Na^+ and CIPs for Mg^{2+} and Ca^{2+}. The agreement between the NMR and DRS ion-pair formation (Fig. 6) supports the above notion that chloride IPs [59,69,75] can be neglected as NMR is only sensitive to the formation of DMP^- IPs, whereas DRS detects all, DMP^- and Cl^- IPs: If the formation of chloride ion-pairs was significant, the DRS equilibrium constants would be overestimated and would be greater than those obtained from NMR, which is not the case. Furthermore, the prevalence of solvent-shared $NaDMP^0$ is also consistent with MD simulations [35,36,40], whereas the dominant formation of CIPs in the case of the bivalent cations is in line with the speciation inferred from spectroscopic studies [39,43,44]. Quantitatively, the calculated degree of ion pairing at the highest concentration of the present work, c_{salt} = 0.4 M, is ∼ 21 % for Mg^{2+} and ∼ 27 % for Ca^{2+}, which is broadly consistent with the range of 23–37 % and 12–30 % reported in Ref. [44] at c_{salt} = 2 M. DFT calculations [37] and vibrational spectra [44] also suggest the formation of CIPs with Na^+ and SIPs for Mg^{2+} and Ca^{2+}. We find no evidence for these species to significantly contribute to the dielectric spectra, which may be explained by their lifetimes being too short to significantly contribute to the dielectric spectra.

The stability constants in Figures 6 and S10 (SI) strongly depend on the ionic strength (I), expressed as:

$$I = \frac{1}{2}\sum_i [X_i] z_i^2 = c_{NaDMP} + m c_{salt} - \frac{m+1}{2}[IP] \quad (9)$$

where $[X_i]$ and z_i denote the equilibrium concentration and charge number of species X_i; m is 1 for NaCl and 3 for $MgCl_2$/$CaCl_2$, respectively. In order to obtain the thermodynamic association constants at infinite dilution, log K^0 at $I \to 0$, we fit log K as a function of I using an extended Guggenheim equation [47]:

$$\log K = \log K^0 - \frac{2A_{DH}|z_+ z_-|\sqrt{I}}{1 + B_{DH} d\sqrt{I}} + aI + bI^{3/2} \quad (10)$$

where A_{DH} = 0.5073 $M^{-1/2}$ and B_{DH} = 3.2823 $M^{-1/2}$ $nm^{-1/2}$ are Debye-Hückel parameters for water at 20 °C, d is the charge distance, a and b are empirical parameters. For each IP, an error-weighted fit of Eq. (10) provides an excellent description of the

log K data (Fig. 6) and parameters of Eq. (10) are listed in Table S7, SI. The calculated log K^0 constants are listed in Table 1 and Table S7, SI. Overall, we find these constants to follow the trend of $Ca^{2+} \approx Mg^{2+} \gg Na^+$, which is in line with what has been found earlier for DMP^- [31], other monophosphates [77], and also nucleic acids [4,6,20–22,28,30].

3.5. Comparison of Mg^{2+}-binding to DMP^- and to phosphate of the RNA's backbone

Given DMP^- is often used as a simple model for studying binding of metal ions to phosphate groups of nucleic acids' backbone, we compare its binding affinity with that of yeast $tRNA^{Phe}$. Recent IR experiments have suggested the formation of 6 ± 2 direct contacts between Mg^{2+} and phosphate at c_{MgCl2}/c_{RNA} = 15 with c_{RNA} = 0.001 M [21]. As each of these RNA molecules has ~ 72 phosphate groups, these direct contacts correspond to 6–11 % of the phosphate moieties forming CIPs with Mg^{2+}.

Using the analogous conditions for solutions of NaDMP (c_{NaDMP} = 0.072 M and c_{MgCl2} = 0.015 M), the log K^0 association constants obtained in this work (Table 1) suggest that 11 % of all phosphate groups form $MgDMP^+$ IPs – in line with the upper limit reported in Ref. [21]. As such, despite this comparison neglects the different chemical structures of RNA and DMP^-, the good agreement between the estimate and the findings for RNA indicates that the binding strength between Mg^{2+} and a single DMP^- can provide a good estimate for the Mg^{2+}-binding affinity of $tRNA^{Phe}$. In turn, the proximity of different chemical moieties to the phosphate groups in RNA, as compared to DMP^- appears to have a small impact on the interaction with metal cations. The similarity of log K^0 for $MgDMP^+$ (1.32) and Mg^{2+}-phosphate for the RNA backbone (1.05) [30] supports this notion.

3.6. The kinetics of ion pairing

In addition to the information on the ion-pairing equilibria obtained from the S_1 solute relaxation strengths (amplitudes), the solute relaxation times, τ_1, provide insights into the dynamics of the IPs: since both species, DMP^- and IP, contribute to the detected relaxation, mode 1 is composed of spectrally unresolved relaxations of DMP^- and IP, with corresponding unresolved relaxation times τ_{DMP} and τ_{IP}. As for diffusive rotation these relaxation times are expected to scale with the volume (V) of the rotating species [45,59], our finding implies that the volumes of the anion and the IP are too similar for the underlying two relaxations to be experimentally disentangled. Based on the notion of mode 1 being a composite one, the observed relaxation time τ_1 is expected to be the amplitude-weighted average of τ_{IP} and τ_{DMP}. As the IP contribution increases in magnitude upon addition of salts to NaDMP (NaCl: up to 0.6–0.8 M, $MgCl_2$ and $CaCl_2$: up to at least 0.4 M, see Fig. 5) and as $\tau_{IP} > \tau_{DMP}$ (owing to $V_{IP} > V_{DMP}$), an increase of τ_1 would be expected. This is in stark contrast to the experimentally determined values of τ_1: The addition of NaCl to solutions of NaDMP results in a decrease in τ_1 (see Figure S10a, SI). Similarly, the addition of $MgCl_2$ or $CaCl_2$, makes τ_1 to decrease with increasing salt concentration, after a minor increase at low concentrations (Figure S10b, SI).

Thus, the observed variation of τ_1 cannot be explained by the varying contributions of DMP and IP according to the chemical equilibria. Yet, also the kinetics of ion pairing can affect relaxation times: If the rate of chemical exchange between the IP and free ions becomes comparable to the rate of dipolar rotation, the IP dissociation dynamics contributes to the observed relaxation time [45,78,79]. These two competing dynamics, dipolar rotation and IP formation/dissociation have been used to explain the decrease in the ion-pair relaxation time with increasing salt concentration observed for simple salts composed of spherical ions [45,72]. This has been achieved by approximating the dissociation rate of the IPs as the rate of chemical relaxation, i.e. the rate of the ion-pairing reaction after deflection from equilibrium [45], despite chemical relaxation also including the rate of IP formation.

To address this apparent contradiction in the model of Refs. [45] and [79] and to also account for the contribution of the dipolar DMP^- ions for our studied samples, we consider here the IP association/dissociation reaction (Eq. (6)) with its equilibrium constant (K) and rate coefficients of IP formation (k_1) and dissociation (k_{-1}) and the ion-pair metathesis with its formation (K^*) and rate constants k_2, k_{-2}:

$$IP + M^* \rightleftharpoons IP^* + M \tag{11}$$

Note that $K = k_1 c^{\circ}/k_{-1}$ (c° is 1 M), whereas $K^* = k_2/k_{-2} = 1$, since $k_2 = k_{-2} = k^*$.

Based on these reaction rates, we obtain the time-correlation function of the macroscopic dipole moment of the samples in analogy to Ref. [79]. The details of the derivation are given in the SI, but in brief: In our approach, the intrinsic IP dissociation rate, k_{-1}, which leads to a decay of the dipolar correlation function, is independent of concentration. In turn, the decrease in K with increasing ionic strength is solely due to a decrease in the IP formation rate, k_1, which one would expect for the association of two charged species (Eq. (6)) based on the kinetic salt effect [80]. The IP metathesis (Eq. (11)) does not affect equilibrium concentrations. Yet, as ion metathesis can randomize the orientation of the dipole moment of the IP, we consider this reaction to be a cause for the loss of dipolar correlations. As such, the overall observed relaxation rates, τ_1^{-1}, depend on the concentration of cations, [M]. We note that also anion metathesis would have the same concentration-dependent effect on dipolar correlations, but for the present samples, we neglect such a process because c_{DMP} is constant, contrary to the large variation of c_M. Based on these equilibria, the observed relaxation rates τ_1^{-1} can be approximated as:

$$\tau_1{}^{-1} = \beta\left(\tau_{IP}{}^{-1} + k_{-1} + k^*[M]\right) + (1-\beta)\left(\tau_{DMP}{}^{-1} + k_1[M]\right) + 2k_{-1}\gamma \tag{12}$$

with.

$$\beta = \frac{[IP]\mu_{IP}{}^2}{[IP]\mu_{IP}{}^2 + [DMP]\mu_{DMP}{}^2} \tag{13}$$

$$\gamma = \frac{[IP]\mu_{IP}\mu_{DMP}}{[IP]\mu_{IP}{}^2 + [DMP]\mu_{DMP}{}^2} \tag{14}$$

Here, τ_{IP} and τ_{DMP} are the rotational correlation times (or intrinsic molecular relaxation times) of the IP and the anion, respectively. The concentration-dependent equilibrium concentrations [IP], [DMP], [M] were calculated according to the fits of the experimental data (Fig. 6) according to Eq. (9) (parameters are listed in Table S7, SI), via refining I as a function of c_{salt} in an iterative process. In addition, the dependence of k_1 on c_{salt} was taken into account as $k_1 = k_{-1}K$. To further reduce the number of adjustable parameters, we set τ_{IP} to the value estimated from the Stokes-Einstein-Debye (SED) equation using the geometric model described in Refs. [76,81], assuming stick boundary conditions for the rotating particle and the viscosity to be the viscosity of neat water at 20 °C [82]. These values for τ_{IP} are given in Table 2. As such, k_{-1}, k^*, and τ_{DMP} are the only adjustable parameters in Eqs. (12)–(14). As can be seen in Fig. 7, Eq. (12) provides an excellent description of the concentration-dependence of τ_1^{-1} for all three salts and the corresponding parameters are listed in Table 2.

These fits suggest that the intrinsic dissociation rate of $NaDMP^0$ is higher than for $CaDMP^+$. For $MgDMP^+$ the fits yielded very small and negative k_{-1} values with large uncertainty. This suggests that

Table 2
Parameters obtained from fitting Eq. (12) to the experimental relaxation rates τ_1^{-1}: rate of dissociation (k_{-1}), rate of metathesis (k^*), and the rotational correlation time of DMP^- (τ_{DMP}). Also listed are the rate of ion-pair formation (k_1) and ion-pair rotational correlation time (τ_{IP}) as determined from the Stokes-Einstein-Debye (SED) equation.

Species	Type of IP	$k_{-1}\cdot10^{-9}$ / s^{-1}	$k_1\cdot10^{-9}$ / $M^{-1}s^{-1}$ [a]	$k^*\cdot10^{-9}$ / $M^{-1}s^{-1}$	τ_{IP} / ps [b]	τ_{DMP} / ps
$NaDMP^0$	SIP	3.0 ± 0.5	2.3 ± 0.6	13.6 ± 0.9	280	99 ± 13
$MgDMP^+$	CIP	0 [b]	0	33.1 ± 0.9	160	47 ± 1
$CaDMP^+$	CIP	1.4 ± 0.4	31.2 ± 1.0	38.2 ± 1.7	176	44 ± 2

[a] Calculated as $k_{-1}K^0$; the log K^0 values are listed in Table 1.
[b] Fixed during fitting.

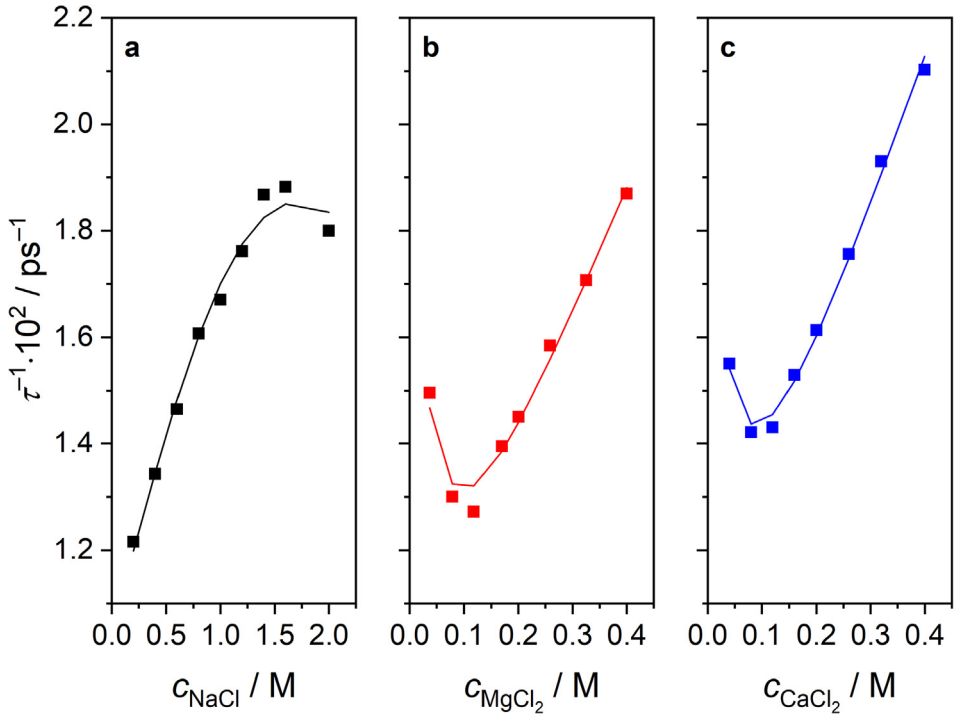

Fig. 7. Inverse relaxation time of the solute mode 1 (τ_1) as a function of the concentration of added **a)** NaCl (average of two data sets), **b)** $MgCl_2$ and **c)** $CaCl_2$. Symbols represent experimental data; solid lines are the results of fitting Eq. (12) to the data.

the dissociation of the $MgDMP^+$ according to Eq. (6) is too slow to significantly affect the detected relaxation rates τ_1^{-1}; thus, we set k_{-1} to 0. The fitted rotational correlation times of DMP^- obtained from the experiments with added $MgCl_2$ and $CaCl_2$ agree well with the values estimated via the SED equation assuming a spherical shape of DMP^- (42 ps), while the fit for the experiments with added NaCl gives a higher value.

We find that the metathesis reaction is important to model the experimental data. Omitting this ion exchange process when fitting Eq. (12) to the data ($k^* = 0$) yields a significantly worse description of the experimental data. As such, our analysis suggests that metathesis is an important mechanism for IP dissociation. Namely, comparison of k_{-1} and $k^*[M]$ shows the latter to be the dominant contribution: $k^*[M] > k_{-1}$ for $NaDMP^0$ ($c_{NaCl} \geq 0.2$ M), $CaDMP^+$ ($c_{CaCl2} \geq 0.08$ M), and $k^*[M] \gg k_{-1}$ for $MgDMP^+$ in the entire concentration range. We find the metathesis rates k^* to be comparable for $CaDMP^+$ and $MgDMP^+$, yet significantly higher for the IPs with divalent cations than for the $NaDMP^0$ species, which may reflect the competition between self-dissociation and metathesis: the lifetime of $NaDMP^0$ is shorter than that of $CaDMP^+$ and $MgDMP^+$ (see below), also suggesting a lower probability of metathesis for the former species.

Overall, the data in Table 2 suggest the IP dissociation rates to follow the order of $Mg^{2+} \ll Ca^{2+} < Na^+$, which reflects most likely the affinity of the metal ions towards DMP^-: phosphate has a preference for binding Mg^{2+} over Ca^{2+}, with the complexation of these ions by ATP [83] being a prominent example. The trend of dissociation rates of DMP^- ion-pairs found here also correlates with the trend for the exchange rates of water molecules in the hydration shells: The average dwelling time of an H_2O molecule in the ions hydration shell is a few microseconds for Mg^{2+}, nanoseconds for Ca^{2+} [84] and picoseconds for Na^+ [85], yielding the same order of dissociation rates.

The corresponding ion-pair lifetimes ($\tau_L = k_{-1}^{-1}$) in the absence of ion metathesis, i.e. [M] → 0, are $\tau_L(NaDMP^0) \approx 330$ ps and $\tau_L(CaDMP^+) \approx 700$ ps, which are in good agreement with the lifetimes of other CIPs forming in water [45,86]. Our results also broadly agree with MD simulations on solutions containing Ca^{2+} and DMP^-, which suggest the lifetime of the CIP to be less than a few nanoseconds [38]. In addition, the negligible dissociation rate of $MgDMP^+$ obtained here, i.e. long residence time of the DMP^- anion in the first coordination shell of Mg^{2+}, is also consistent with the notion that Mg^{2+} ions forming contact pairs with the phosphate groups of $tRNA^{Phe}$ have residence times longer than 1 μs [21]. As such, our results provide a direct experimental estimate for the lifetimes of CIPs in solution, which have been inferred only from MD simulations to date.

4. Conclusions

In this contribution, we study the hydration of the dimethyl phosphate ion (DMP^-) and its ion binding in the presence of NaCl,

$MgCl_2$, or $CaCl_2$ applying dielectric relaxation and nuclear magnetic resonance spectroscopies. For all solutions, the dielectric spectra can be well described by three relaxation modes: two faster processes ascribed to the dipolar reorientation of water, while the slowest mode centered at 2–3 GHz arises from the rotation of solute species. From an analysis of the water relaxation, we find DMP^- to be weakly hydrated. Analysis of the solute mode in the absence of added salts is broadly consistent with rotation of dipolar DMP^- in its gauche-gauche conformation to dominate this relaxation.

Upon addition of salt, we find evidence for the association of Na^+, Mg^{2+}, and Ca^{2+} ions with DMP^-, which increasingly contributes to the solute relaxation. Comparison of the ion-pair concentrations as obtained from the dielectric data to ion association as obtained from NMR chemical shift experiments suggests that contact ion-pairs prevail for Mg^{2+} and Ca^{2+}, whereas solvent-shared ion-pairs dominate ion association in the presence of Na^+. The determined standard association constants follow the order $Ca^{2+} \approx Mg^{2+} > Na^+$ and allow for estimating ion association for a wide range of salt concentrations. Comparison to literature reports demonstrates that such estimates even predict the association of cations to the chemically very dissimilar yeast $tRNA^{Phe}$ very well, suggesting that DMP^- is a good proxy for the phosphate backbone of nucleic acids.

The concentration-dependence of detected solute dipolar reorientation times provides evidence for the contribution of ion-pair dissociation kinetics to the observed relaxation. We model the observed relaxation rates by accounting for cation metathesis and ion-pair dissociation. Based on this model, we find the IP lifetimes for $MgDMP^+$ to be the longest, whereas the lifetimes of $CaDMP^+$ (~700 ps) and of $NaDMP^0$ (~330 ps) are significantly shorter. As such, our results help in narrowing down the so far broad ranges of reported ion-pair lifetimes. Overall, our results on ion association with DMP^- may help to obtain a molecular-level understanding of ion-phosphate association in more complex macromolecular environments.

CRediT authorship contribution statement

Bence Kutus: Conceptualization, Methodology, Software, Formal analysis, Investigation, Data curation, Writing – original draft, Writing – review & editing, Visualization. **Kenneth Wagner:** Software, Validation, Formal analysis, Investigation, Data curation, Writing – review & editing. **Manfred Wagner:** Methodology, Data curation, Formal analysis, Writing – review & editing. **Johannes Hunger:** Conceptualization, Methodology, Formal analysis, Resources, Writing – review & editing, Project administration, Funding acquisition.

Data availability

Data will be made available on request.

Declaration of Competing Interest

The authors declare that they have no known competing financial interests or personal relationships that could have appeared to influence the work reported in this paper.

Acknowledgements

The authors express their gratitude to Prof. Dr. Richard Buchner and Dr. Maksim Grechko for helpful discussions, to Prof. Dr. Mischa Bonn for insightful comments on the manuscript and to Christian Muth for his assistance in sample preparation. The help of Katharina Maisenbacher in preparing the graphical abstract is greatly appreciated. B.K. gratefully acknowledges financial support from the Alexander von Humboldt Foundation (grant no. 1209539). J. H. acknowledges funding from the European Research Council (ERC) under the European Union's Horizon 2020 research and innovation program (grant agreement no. 714691)

Appendix A. Supplementary material

Supplementary data to this article can be found online at https://doi.org/10.1016/j.molliq.2022.119868.

References

[1] G.S. Manning, Limiting Laws and Counterion Condensation in Polyelectrolyte Solutions I. Colligative Properties, J. Chem. Phys. 51 (1969) 924–933, https://doi.org/10.1063/1.1672157.
[2] B. Jayaram, B.L. Beveridge, Modeling DNA in Aqueous Solutions: Theoretical and Computer Simulation Studies on the Ion Atmosphere of DNA, Annu. Rev. Biophys. Biomol. Struct. 25 (1996) 367–394, https://doi.org/10.1146/annurev.bb.25.060196.002055.
[3] D.E. Draper, D. Grielly, A.M. Soto, Ions and RNA Folding, Annu. Rev. Biophys. Biomol. Struct. 34 (2005) 221–243, https://doi.org/10.1146/annurev.biophys.34.040204.144511.
[4] Y. Bai, M. Greenfeld, K.J. Travers, V.B. Chu, J. Lipfert, S. Doniach, D. Herschlag, Quantitative and Comprehensive Decomposition of the Ion Atmosphere around Nucleic Acids, J. Am. Chem. Soc. 129 (2007) 14981–14988, https://doi.org/10.1021/ja075020g.
[5] J. Müller, Functional Metal Ions in Nucleic Acids, Metallomics 2 (2010) 318–327, https://doi.org/10.1039/c000429d.
[6] J. Yoo, A. Aksimentiev, Competitive Binding of Cations to Duplex DNA Revealed through Molecular Dynamics Simulations, J. Phys. Chem. B 116 (2012) 12946–12954, https://doi.org/10.1021/jp306598y.
[7] J. Lipfert, S. Doniach, R. Das, D. Herschlag, Understanding Nucleic Acid-Ion Interactions, Annu. Rev. Biochem. 83 (2014) 813–841, https://doi.org/10.1146/annurev-biochem-060409-092720.
[8] S.A. Woodson, Metal Ions and RNA folding: A Highly Charged Topic with a Dynamic Future, Curr. Opin. Chem. Biol. 9 (2005) 104–109, https://doi.org/10.1016/j.cbpa.2005.02.004.
[9] Z.-J. Tan, S.-J. Chen, Importance of Diffuse Metal Ion Binding to RNA, in: A. Sigel, H. Sigel, R.K.O. Sigel (Eds.), Metal Ions in Life Sciences, Vol. 9, Royal Society of Chemistry, Cambridge, 2011, pp. 101–124, https://doi.org/10.1039/9781849732512-00101.
[10] H. Rosenbach, J. Borggräfe, J. Victor, C. Wuebbe, O. Schiemann, W. Hoyer, G. Steger, M. Etzkorn, I. Span, Influence on Monovalent Metal Ions on Metal Binding and Catalytic Activity of the 10–23 DNAzyme, Biol. Chem. 402 (2021) 99–111, https://doi.org/10.1515/hsz-2020-0207.
[11] G. Palermo, A. Cavalli, M.L. Klein, M. Alfonso-Prieto, M. Dal Peraro, M. De Vivo, Catalytic Metal Ions and Enzymatic Processes of DNA and RNA, Acc. Chem. Res. 48 (2015) 220–228, https://doi.org/10.1021/ar500314j.
[12] Z. Yang, J.J. Hayes, The Divalent Cations Ca^{2+} and Mg^{2+} Play Specific Roles in Stabilizing Histone–DNA Interactions within Nucleosomes That Are Partially Redundant with the Core Histone Tail Domains, Biochem. 50 (2011) 9973–9981, https://doi.org/10.1021/bi201377x.
[13] H.J. Shi, P.B. Moore, The Crystal Structure of Yeast Phenylalanine tRNA at 1.93 Angstrom Resolution: A Classic Structure Revisited, RNA 6 (2000) 1091–1110, https://doi.org/10.1017/S1355838200000364.
[14] M. Egli, DNA-Cation Interactions: Quo Vadis?, Chem Biol. 9 (2002) 277–286, https://doi.org/10.1016/S1074-5521(02)00116-3.
[15] D.J. Klein, P.B. Moore, T.A. Steitz, The Contribution of Metal Ions to the Structural Stability of the Large Ribosomal Subunit, RNA 10 (2014) 1366–1379, https://doi.org/10.1261/rna.7390804.
[16] S.P. Meisburger, S.A. Pabit, L. Pollack, Determining the Locations or Ions and Water around DNA from X-Ray Scattering Measurements, Biophys. J. 108 (2015) 2886–2895, https://doi.org/10.1016/j.bpj.2015.05.006.
[17] F. Leonarski, L. D'Ascenzo, P. Auffinger, Mg^{2+} Ions: Do They Bind to Nucleobase Nitrogens?, Nucl Acids Res. 45 (2017) 987–1004, https://doi.org/10.1093/nar/gkw1175.
[18] J.A. Cowan, Coordination Chemistry of Mg^{2+} and 5S rRNA (Escherichia coli): Binding Parameters, Ligand Symmetry, and Implications for Activity, J. Am. Chem. Soc. 113 (1991) 675–676, https://doi.org/10.1021/ja00002a046.
[19] B. Fürtig, C. Richter, J. Wöhnert, H. Schwalbe, NMR Spectroscopy of RNA, ChemBioChem 4 (2003) 936–962, https://doi.org/10.1002/cbic.200300700.
[20] S. K. Kolev, P. St. Petkov, M. A. Rangelov, D. V. Trifonov, T. I. Milenov, G. N. Vayssilov, Interaction of Na^+, K^+, Mg^{2+} and Ca^{2+} Counter Cations with RNA, Metallomics 10 (2018) 659–678. https://doi.org/10.1039/C8MT00043C.
[21] J. Schauss, A. Kundu, B.P. Fingerhut, T. Elsaesser, Magnesium Contact Ions Stabilize the Tertiary Structure of Transfer RNA: Electrostatics Mapped by Two-Dimensional Infrared Spectra and Theoretical Simulations, J. Phys. Chem. B 125 (2021) 740–747, https://doi.org/10.1021/acs.jpcb.0c08966.
[22] N. Korolev, A.P. Lyubartsev, A. Rupprecht, L. Nordenskiöld, Competitive Binding of Mg^{2+}, Ca^{2+}, Na^+ and K^+ Ions to DNA in Oriented DNA Fibers:

Experimental and Monte Carlo Simulation Results, Biophys. J. 77 (1999) 2736–2749, https://doi.org/10.1016/S0006-3495(99)77107-9.
[23] M. Feig, B.M. Pettitt, Sodium and Chlorine Ions as Part of the DNA Solvation Shell, Biophys. J. 77 (1999) 1769–1781, https://doi.org/10.1016/j.cellbi.2008.03.002.
[24] P. Várnai, K. Zakrzewska, DNA and Its Counterions: A Molecular Dynamics Study, Nucl. Acids Res. 32 (2004) 4269–4280, https://doi.org/10.1093/nar/gkh765.
[25] Y. Cheng, N. Korolev, L. Nordenskiöld, Similarities and Differences in Interaction of K^+ and Na^+ with Condensed Ordered DNA. A Molecular Dynamics Computer Simulation Study, Nucl. Acids Res. 34 (2006) 686–696, https://doi.org/10.1093/nar/gkj434.
[26] R.L. Hayes, J.K. Noel, U. Mohanty, P.C. Whitford, S.C. Hennelly, J.N. Onuchic, K.Y. Sanbonmatsu, Magnesium Fluctuations Modulate RNA Dynamics in the SAM-I Riboswitch, J. Am. Chem. Soc. 134 (2012) 12043–12053, https://doi.org/10.1021/ja301454u.
[27] F. Pan, C. Roland, C. Sagui, Ion Distributions Around Left- and Right-Handed DNA and RNA Duplexes: A Comparative Study, Nucl. Acids Res. 42 (2014) 13981–13996, https://doi.org/10.1093/nar/gku1107.
[28] M.P. Long, S. Alland, M.E. Martin, C.M. Isborn, Molecular Dynamics Simulations of Alkaline Earth Metal Ions Binding to DNA reveal Ion Size and Hydration Effects, Phys. Chem. Chem. Phys. 22 (2020) 5584–5596, https://doi.org/10.1039/C9CP06844A.
[29] H.T. Nguyen, D. Thirumalai, Charge Density of Cation Determines Inner versus Outer Shell Coordination to Phosphate in RNA, J. Phys. Chem. B 124 (2020) 4114–4122, https://doi.org/10.1021/acs.jpcb.0c02371.
[30] R.K.O. Sigel, H. Sigel, A Stability Concept for Metal Ion Coordination to Single-Stranded Nucleic Acids and Affinities of Individual Sites, Acc. Chem. Res. 43 (43) (2010) 974–984, https://doi.org/10.1021/ar900197y.
[31] P. Haake, R.V. Prigodich, Method for Determination of Phosphate Anion-Cation Association Constants form ^{31}P Chemical Shifts, Inorg. Chem. 23 (1984) 457–462, https://doi.org/10.1021/ic00172a017.
[32] D. Hadži, M. Hodošček, J. Grdadolnik, F. Avbelj, Intermolecular Effects on Phosphate Frequencies in Phospholipids – Infrared Study and Ab-Initio Model Calculation, J. Mol. Struct. 266 (1992) 9–19, https://doi.org/10.1016/0022-2860(92)80046-K.
[33] Y. Guan, C. J. Wurrey, G. J. Thomas, Jr., Vibrational Analysis of Nucleic Acids. 1. The Phosphodiester Group in Dimethyl Phosphate Model Compounds: $(CH_3O)_2PO_2^-$, $(CD_3O)_2PO_2^-$, and $(^{13}CH_3O)_2PO_2^-$, Biophys. J. 66 (1994) 225–235. https://doi.org/10.1016/S0006-3495(94)80767-2.
[34] J. Florián, V. Baumruk, M. Štrajbl, L. Bednárová, J. Štěpánek, IR and Raman Spectra, Conformational Flexibility, and Scaled Quantum Mechanical Force Fields of Sodium Dimethyl Phosphate and Dimethyl Phosphate Anion, J. Phys. Chem. 100 (1996) 1559–1568, https://doi.org/10.1021/jp9520299.
[35] S.E. Huston, P.J. Rossky, Free Energies of Association for the Sodium-Dimethyl Phosphate Ion Pair in Aqueous Solution, J. Phys. Chem. 93 (1999) 7888–7895, https://doi.org/10.1021/j100360a031.
[36] E. Schwegler, G. Galli, F. Gygi, Conformational Dynamics of the Dimethyl Phosphate Anion in Solution, Chem. Phys. Lett. 342 (2001) 434–440, https://doi.org/10.1016/S0009-2614(01)00604-2.
[37] A.S. Petrov, J. Funseth-Smotzer, G.R. Pack, Computational Study of Dimethyl Phosphate Anion and Its Complexes with Water, Magnesium, and Calcium, Int. J. Quantum Chem. 102 (2005) 645–655, https://doi.org/10.1002/qua.20442.
[38] J.J. Potoff, Z. Issa, C.W. Manke Jr., B.P. Jena, Ca^{2+}–Dimethylphosphate Complex Formation: Providing Insight into Ca^{2+}–Mediated Local Dehydration and Membrane Fusion in Cells, Cell Biol. Int. 32 (2008) 361–366, https://doi.org/10.1016/j.cellbi.2008.03.002.
[39] E.L. Christian, V.E. Anderson, P.R. Carey, M.E. Harris, A Quantitative Raman Spectroscopic Signal for Metal-Phosphodiester Interactions in Solution, Biochem. 49 (2010) 2869–2879, https://doi.org/10.1021/bi901866u.
[40] P. Ganguly, P. Schravendijk, B. Hess, N.F.A. van der Vegt, Ion Pairing in Aqueous Electrolyte Solutions with Biologically Relevant Anions, J. Phys. Chem. B 111 (2015) 3734–3739, https://doi.org/10.1021/jp201150q.
[41] C. Zhang, C. Lu, Q. Wang, J. W. Ponder, P. Ren, Polarizable Multipole-Based Force Field for Dimethyl and Trimethyl Phosphate, J. Chem. Theor. Comp. 11 (2015) 5326–5339. https://doi.org/10.1021/acs.jctc.5b00562.
[42] M.T. Panteva, G.M. Giambaşu, D.M. York, Force Field for Mg^{2+}, Mn^{2+}, Zn^{2+}, and Cd^{2+} Ions That Have Balanced Interactions with Nucleic Acids, J. Phys. Chem. B 119 (2015) 15460–15470, https://doi.org/10.1021/acs.jpcb.5b10423.
[43] J. Schauss, F. Dahms, B.P. Fingerhut, T. Elsaesser, Phosphate-Magnesium Interactions in Water Probed by Ultrafast Two-Dimensional Infrared Spectroscopy, J. Phys. Chem. Lett. 10 (2019) 238–243, https://doi.org/10.1021/acs.jpclett.8b03568.
[44] J. Schauss, A. Kundu, B.P. Fingerhut, T. Elsaesser, Contact Ion Pairs of Phosphate Groups in Water: Two-Dimensional Infrared Spectroscopy of Dimethyl Phosphate and Ab Initio Simulations, J. Phys. Chem. Lett. 10 (2019) 6281–6286, https://doi.org/10.1021/acs.jpclett.9b02157.
[45] R. Buchner, J. Barthel, Kinetic Processes in the Liquid Phase Studied by High-Frequency Permittivity Measurements, J. Mol. Liq. 63 (1995) 55–75, https://doi.org/10.1016/0167-7322(95)92021-3.
[46] Y. Marcus, G. Hefter, Ion Pairing, Chem. Rev. 106 (2006) 4585–4621, https://doi.org/10.1021/cr040087x.
[47] R. Buchner, G. Hefter, Interactions and Dynamics in Electrolyte Solutions by Dielectric Spectroscopy, Phys. Chem. Chem. Phys. 11 (2009) 8984–8999. DOI https://doi.org/10.1039/B906555P.
[48] W.D. Kumler, J.J. Eiler, The Acid Strength of Mono and Diesters of Phosphoric Acid. The n-Alkyl Esters from Methyl to Butyl, the Esters of Biological Importance, and the Natural Guanidine Phosphoric Acids, J. Am. Chem. Soc. 65 (1943) 2355–2361, https://doi.org/10.1021/ja01252a028.
[49] F. Kremer, A. Schönhals, in: Broadband Dielectric Spectroscopy, Springer, Berlin-Heidelberg, 2003, pp. 1–33.
[50] J. Hunger, Effects of Polar Compounds on the Dynamics and Dielectric Properties of Room-Temperature Ionic Liquids, University of Regensburg, Regensburg, 2009, PhD Thesis.
[51] S. Schrödle, Effects of Non-Ionic Surfactants and Related Compounds on the Cooperative and Molecular Dynamics of Their Aqueous Solutions, University of Regensburg, Regensburg, 2005, PhD Thesis.
[52] Y. Zhao, D.G. Truhlar, The M06 suite of Density Functionals for Main Group Thermochemistry, Thermochemical Kinetics, Noncovalent Interactions, Excited States, and Transition Elements: Two New Functionals and Systematic Testing of Four M06-Class Functionals and 12 Other Functionals, Theor. Chem. Acc. 120 (2008) 215–241, https://doi.org/10.1007/s00214-007-0310-x.
[53] F. Weigend, R. Ahlrichs, Balanced Basis Sets of Split Valence, Triple Zeta Valence and Quadruple Zeta Valence Quality for H to Rn: Design and Assessment of Accuracy, Phys. Chem. Chem. Phys. 7 (2005) 3297–3305, https://doi.org/10.1039/B508541A.
[54] S. Grimme, J. Antony, S. Ehrlich, H.A. Krieg, Consistent and accurate ab initio parametrization of density functional dispersion correction (DFT-D) for the 94 elements H-Pu, J. Chem. Phys. 132 (2010), https://doi.org/10.1063/1.3382344 154104.
[55] Gaussian 09, Revision D.01., Gaussian, Inc., Wallingford, 2009.
[56] M. Cossi, N. Rega, G. Scalmani, V. Barone, Energies, Structures, and Electronic Properties of Molecules in Solution with the C-PCM Solvation Model, J. Comp. Chem. 24 (2003) 669–681, https://doi.org/10.1002/jcc.10189.
[57] R. Buchner, J. Barthel, J. Stauber, The Dielectric Relaxation of Water Between 0 °C and 35°C, Chem. Phys. Lett. 306 (1999) 57–63, https://doi.org/10.1016/S0009-2614(99)00455-8.
[58] D.A. Turton, J. Hunger, G. Hefter, R. Buchner, K. Wynne, Glasslike Behavior in Aqueous Electrolyte Solutions, J. Chem. Phys. 128 (16) (2008) 161102.
[59] A. Eiberweiser, R. Buchner, Ion-pair or Ion-Cloud Relaxation? On the Origin of Small-Amplitude Low-Frequency Relaxations of Weakly Associating Aqueous Electrolytes, J. Mol. Liq. 176 (2012) 52–59, https://doi.org/10.1016/j.molliq.2012.03.025.
[60] I. Popov, P.B. Ishai, A. Khamzin, Y. Feldman, The Mechanism of the Dielectric Relaxation of Water, Phys. Chem. Chem. Phys. 18 (2016) 13941–13953, https://doi.org/10.1039/C6CP02195F.
[61] V. Balos, S. Imoto, R.R. Netz, M. Bonn, D.J. Bonthuis, Y. Nagata, J. Hunger, Macroscopic Conductivity of Aqueous Electrolyte Solutions Scales with Microscopic Ion Motions, Nat. Commun. 11 (2020) 1611, https://doi.org/10.1038/s41467-020-15450-2.
[62] S. Sega, S. Kantorovich, A. Arnold, Kinetic Dielectric Decrement Revisited: Phenomenology of Finite Ion Concentrations, Phys. Chem. Chem. Phys. 17 (2015) 130–133, https://doi.org/10.1039/C4CP04182H.
[63] K.F. Rinne, S. Gekle, R.R. Netz, Ion-Specific Solvation Water Dynamics: Single Water versus Collective Water Effects, J. Phys. Chem. A 118 (2014) 11667–11677, https://doi.org/10.1021/jp5066874.
[64] R. Cota, N. Ottosson, H.J. Bakker, S. Woutersen, Evidence for Reduced Hydrogen Bond Cooperativity in Ionic Solvation Shells from Isotope-Dependent Dielectric Relaxation, Phys. Rev. Lett. 120 (2018), https://doi.org/10.1103/PhysRevLett.120.216001 216001.
[65] J. Hunger, S. Niedermayer, R. Buchner, G. Hefter, Are Nanoscale Ion Aggregates Present in Aqueous Solutions of Guanidinium Salts?, J Chem. Phys. B 14 (2010) 13617–13627, https://doi.org/10.1021/jp101520h.
[66] C. Rønne, L. Thrane, P.-O. Åstrand, A. Wallqvist, K.V. Mikkelsen, S. Keiding, Low Frequency Spectroscopy of Liquid Water Using THz-Time Domain Spectroscopy, J. Chem. Phys. 107 (1997) 5319–5331, https://doi.org/10.1016/S0167-7322(02)00093-4.
[67] H. Yada, M. Nagai, K. Tanaka, Origin of the Fast Relaxation Component of Water and Heavy Water Revealed by Terahertz Time-Domain Attenuated Total Reflection Spectroscopy, Chem. Phys. Lett. 464 (2009) 166–170, https://doi.org/10.1016/j.cplett.2008.09.015.
[68] J.T. Kindt, C. Schuttenmaer, Far-Infrared Dielectric Properties of Polar Liquids Probed by Femtosecond Terahertz Pulse Spectroscopy, J. Phys. Chem. 100 (1996) 10373–10379, https://doi.org/10.1021/jp960141g.
[69] S. Friesen, G. Hefter, R. Buchner, Cation Hydration and Ion Pairing in Aqueous Solutions of $MgCl_2$ and $CaCl_2$, J. Phys. Chem. B 123 (2019) 891–900, https://doi.org/10.1021/acs.jpcb.8b11131.
[70] J. Hubbard, L. Onsager, Dielectric Dispersion and Dielectric Friction in Electrolyte Solutions, J. Chem. Phys. 67 (1977) 4850–4857, https://doi.org/10.1063/1.434664.
[71] Y. Marcus, Ion Properties, Marcel Dekker, New York, 1997.
[72] J. Barthel, H. Hetzenauer, R. Buchner, Dielectric Relaxation of Aqueous Electrolyte Solutions 11. Ion-Pair Relaxation of 1:2, 2:1, and 2:2 Electrolytes, Ber. Bunsenges. Phys. Chem. 96 (1992) 1424–1432, https://doi.org/10.1002/bbpc.19920961015.
[73] A.M. Schrader, S.H. Donaldson Jr., J. Song, C.-Y. Cheng, D.W. Lee, S. Han, J.N. Israelachvili, Correlating Steric Hydration Forces with Water Dynamics Through Surface Force and Diffusion NMR Measurements in a Lipid–DMSO–H_2O System, Proc. Natl. Acad. Sci. 112 (2015) 10708–10713, https://doi.org/10.1073/pnas.1512325112.

[74] A. Eiberweiser, A. Nazet, G. Hefter, R. Buchner, Ion Hydration and Association in Aqueous Potassium Phosphate Solutions, J. Phys. Chem. B 119 (2015) 5270–5281, https://doi.org/10.1021/acs.jpcb.5b01417.
[75] A. De Robertis, C. Rigano, S. Sammartano, O. Zerbinati, Ion Association of Cl^- with Na^+, K^+, Mg^{2+} and Ca^{2+} in Aqueous Solution at $10 \leq T \leq 45$ °C and $0 \leq I \leq$ mol/L: A Literature Data Analysis, Thermochim. Acta 115 (1987) 241–248, https://doi.org/10.1016/0040-6031(87)88370-3.
[76] A. Eiberweiser, Hydration and Ion Pairing of Aqueous Phosphate Solutions as Observed by Dielectric Spectroscopy, University of Regensburg, Regensburg, 2013, PhD Thesis.
[77] S.S. Massoud, H. Sigel, Metal Ion Coordinating Properties of Pyrimidine-Nucleoside S'-Monophosphates (CMP, UMP, TMP) and of Simple Phosphate Monoesters, Including D-Ribose 5-Monophosphate. Establishment of Relations between Complex Stability and Phosphate Basicity, Inorg. Chem. 27 (1988) 1447–1453, https://doi.org/10.1021/ic00281a030.
[78] G. Schwarz, Dielectric Relaxation Due to Chemical Rate Processes, J. Phys. Chem. 71 (1967) 4021–4030, https://doi.org/10.1021/j100871a045.
[79] G. Williams, Correlation Function Treatment of the Dielectric Relaxation of Model Systems Capable of Chemical Relaxation, Adv. Mol. Relaxation Processes 1 (1970) 409–422, https://doi.org/10.1016/0001-8716(70)80003-7.
[80] J.N. Brönsted, C.E. Teeter Jr., On Kinetic Salt Effect, J. Phys. Chem. 28 (1924) 579–587, https://doi.org/10.1021/j150240a003.
[81] J.L. Dote, D. Kivelson, Hydrodynamic Rotational Friction Coefficients for Nonspheroidal Particles, J. Phys. Chem. 87 (1983) 3889–3893, https://doi.org/10.1021/j100243a020.
[82] C.H. Cho, J. Urquidi, S. Singh, G.W. Robinson, Thermal Offset Viscosities of Liquid H_2O, D_2O and T_2O, J. Phys. Chem. B 103 (1999) 1991–1994, https://doi.org/10.1021/jp9842953.
[83] S.M. Shanbhag, G.R. Choppin, Thermodynamics of Mg and Ca Complexation with AMP, ADP, ATP, Inorg. Chim. Acta 138 (1987) 187–192, https://doi.org/10.1016/0003-9861(74)90288-4.
[84] J.P. Larentzos, L.J. Criscenti, A Molecular Dynamics Study of Alkaline Earth Metal-Chloride Complexation in Aqueous Solution, J. Phys. Chem. B 112 (2008) 14243–14250, https://doi.org/10.1021/jp802771w.
[85] S. Kerisit, K.M. Rosso, Transition Path Sampling of Water Exchange Rates and Mechanisms Around Aqueous Ions, J. Chem. Phys. 131 (11) (2009) 114512.
[86] R. Buchner, C. Hölzl, J. Stauber, J. Barthel, Dielectric Spectroscopy of Ion-Pairing and Hydration in Aqueous Tetra-n-Alkylammonium Halide Solutions, Phys. Chem. Chem. Phys. 4 (2002) 2169–2179, https://doi.org/10.1039/B110361J.